



HAL
open science

Characteristics of different charge transfer modes in upward flashes inferred from simultaneously measured currents and fields

Lixia He, Mohammad Azadifar, Quanxin Li, Marcos Rubinstein, Vladimir Rakov, Arturo Mediano, Davide Pavanello, Farhad Rachidi

► **To cite this version:**

Lixia He, Mohammad Azadifar, Quanxin Li, Marcos Rubinstein, Vladimir Rakov, et al.. Characteristics of different charge transfer modes in upward flashes inferred from simultaneously measured currents and fields. *High Voltage*, 2020, 5, pp.30 - 37. 10.1049/hve.2019.0017 . hal-03586357

HAL Id: hal-03586357

<https://hal.science/hal-03586357>

Submitted on 23 Feb 2022

HAL is a multi-disciplinary open access archive for the deposit and dissemination of scientific research documents, whether they are published or not. The documents may come from teaching and research institutions in France or abroad, or from public or private research centers.

L'archive ouverte pluridisciplinaire **HAL**, est destinée au dépôt et à la diffusion de documents scientifiques de niveau recherche, publiés ou non, émanant des établissements d'enseignement et de recherche français ou étrangers, des laboratoires publics ou privés.



Distributed under a Creative Commons Attribution - NonCommercial - NoDerivatives 4.0 International License

Characteristics of different charge transfer modes in upward flashes inferred from simultaneously measured currents and fields

eISSN 2397-7264
 Received on 29th January 2019
 Revised 22nd April 2019
 Accepted on 24th May 2019
 doi: 10.1049/hve.2019.0017
 www.ietdl.org

Lixia He^{1,2}, Mohammad Azadifar^{1,3}, Quanxin Li^{1,4}, Marcos Rubinstein³, Vladimir A. Rakov^{5,6}, Arturo Mediano⁷, Davide Pavanello⁸, Farhad Rachidi¹ ✉

¹Electromagnetic Compatibility Laboratory, Swiss Federal Institute of Technology (EPFL), 1015 Lausanne, Switzerland

²Department of Atmospheric Physics, Nanjing University of Information Science and Technology, Nanjing, People's Republic of China

³University of Applied Sciences of Western Switzerland (HES-SO), 1400 Yverdon-les-Bains, Switzerland

⁴Department of Electrical Engineering, Wuhan University, Wuhan, People's Republic of China

⁵Department of Electrical and Computer Engineering, University of Florida, Florida, USA

⁶Institute of Electronics and Mathematics, National Research University Higher School of Economics, Moscow, Russia

⁷Department Electronics and Communication Engineering, University of Zaragoza, Zaragoza, Spain

⁸Institute of Sustainable Energy, University of Applied Sciences of Western Switzerland (HES-SO), 1950 Sion, Switzerland

✉ E-mail: farhad.rachidi@epfl.ch

Abstract: The authors present an analysis of different charge transfer modes during upward negative flashes. The analysis includes a total number of 94 pulses that occurred during two upward negative flashes recorded at the Säntis Tower. The pulses included 59 mixed-mode (MM) initial continuous current (ICC) pulses, 17 M-component-type ICC (M-ICC) pulses, 8 return-stroke pulses, and 10 classical M-component (MC) pulses. It is found that the initial stage of the flash is responsible for the largest share of the total charge transferred to the ground. Simulation results for the electric fields associated with the considered charge transfer modes are presented and discussed. Return stroke (RS) and MM pulses were simulated adopting the MTLE model, while MCs and M-ICC pulses were simulated using the guided wave model of Rakov *et al.* The simulated results are shown to be in good agreement with simultaneous records of electric fields measured at a distance of 15 km from the Säntis Tower. The inferred velocities for MCs and M-ICC pulses range from 2.0×10^7 to 9.0×10^7 m/s, and the corresponding junction point heights range from 1.0 to 2.0 km. The inferred pulse velocities for RSs and MM pulses range from 1.3×10^8 to 1.65×10^8 m/s. The inferred current attenuation constants of the MTLE model obtained in this study range from 0.3 to 0.8 km, lower than the value of 2 km previously suggested for RSs in downward flashes. The obtained results support the assumption that the mode of charge transfer to the ground giving rise to MM pulses is similar to that of RSs. The results are also in support of the generally assumed similarity between M-ICC pulses and classical MCs.

1 Introduction

An M-component (MC) is a transient process occurring during the continuing current (CC) following return strokes (RSs), and it has been studied for more than eight decades (e.g. [1–3]). MCs have distinct characteristics in terms of their current peak; their rise-time and the associated E-field waveforms, significantly different from those associated with the charge transfer in RSs [2]. A typical MC is characterised by a more or less symmetrical current waveform with lower magnitude, much longer rise time and less transferred charge than those for a typical RS. A statistical analysis on the duration, average peak current, and charge transfer during MC current pulses and the preceding CC was presented in [4].

Recently, He *et al.* [5] identified four types of pulses in upward negative flashes observed at the Säntis Tower, namely (i) RSs, which occur after the extinction of the initial continuous current (ICC), if any, and are preceded by an essentially no-current interval, (ii) the so-called mixed-mode (MM) pulses [6], which are fast pulses superimposed on the ICC and are presumably due to the reactivation of a decayed branch or the connection of a newly-created channel to the ICC-carrying channel at low junction heights, with characteristics similar to those of RSs [7], (iii) MC mode pulses superimposed on the CC after some RSs, and (iv) MC-type ICC (M-ICC) pulses, presumably associated with the reactivation of a decayed branch or the connection of a newly-created channel to the ICC-carrying channel at large junction heights [6].

In this study, which is an extension of that presented in [8], we examine the characteristics of different charge transfer modes

associated with two upward flashes initiated at the Säntis Tower in Switzerland. The data are also used as a reference for model-predicted fields. The rest of the paper is organised as follows. Section 2 briefly describes the instrumentation, the dataset, and the methodology. Section 3 presents an analysis of the characteristics of different charge transfer modes using the considered data. Model-predicted results and their comparison with experimental data are presented and discussed in Section 4. The paper ends with a summary and conclusions presented in Section 5.

2 Instrumentation, dataset, and methodology

2.1 Lightning current and E-field measurement system

The Säntis Tower was instrumented in May 2010 for lightning measurements. The tower experimental setup contains two sets of measuring equipment mounted at two heights along with the tower, 24 and 82 m above ground level, each including a Rogowski coil and a multi-gap B-Dot sensor [9]. The measured signals are relayed to a National Instruments PXI-5122 high-speed digitizer (50 MS/s) by means of a fibre-optic link. The measurement window is 2.4 s [9, 10].

An electric field measurement system is located about 15 km away from the Säntis Tower, installed on the roof of a 25-m tall building in Herisau. It comprises a flat plate antenna and an analogue integrator with an overall frequency bandwidth of 30 Hz–2 MHz. The signal is digitised and recorded using a PCI-5122 digitizer with a sampling rate of 5 MS/s and a time window of 4 s.

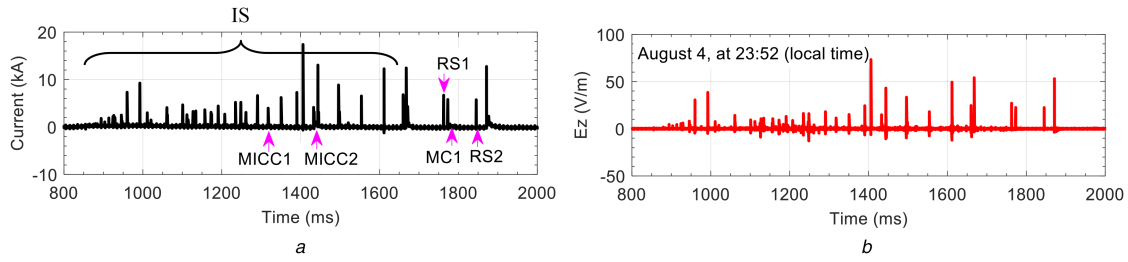


Fig. 1 Overall current and electric field waveforms measured at 15 km

(a) Current, (b) Electric field. The waveforms are associated with an upward negative flash initiated from the Sántis Tower on 4 August, at 23:52. The pink arrows in the left panel show five of the eight pulses used in Section 4

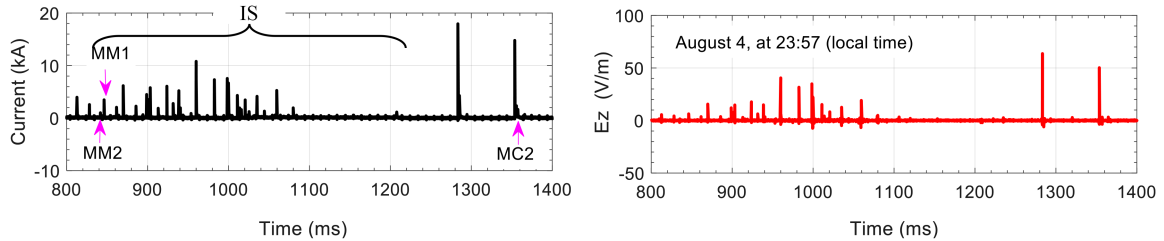


Fig. 2 Same as in Fig. 1, but for a flash that occurred on 4 August, at 23:57. The pink arrows in the left panel show three of the eight pulses used in Section 4

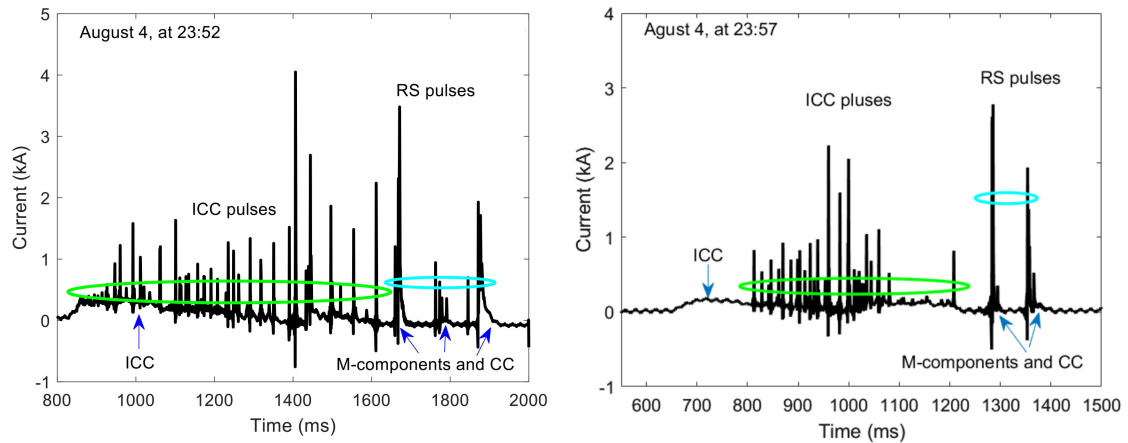


Fig. 3 Current waveforms of the two considered flashes after filtering with a 1-kHz low-pass, zero-phase filter to accentuate the slower varying ICC and the CC. The green coloured ellipse groups the ICC pulses and the cyan blue coloured ellipse groups the RSs and MCs pulses

2.2 Dataset and methodology

The dataset is composed of simultaneous records of currents and E-field waveforms associated with pulses belonging to two upward negative flashes initiated from the Sántis Tower on 4 August 2016, at 23:52 and at 23:57 (local time).

A total of 94 pulses (including ICC pulses and RSs) in our data set were classified into four categories according to the approach proposed in [5]. A brief description of the considered four categories of pulses is in order. The initial stage in upward negative flashes consists of an upward positive leader followed by an ICC lasting typically a few hundreds of milliseconds. RS pulses are pulses that appear after the extinction of the ICC, if any, immediately preceded by an essentially no-current interval. During the initial stage, two types of pulses can be superimposed to the ICC. Pulses of the first type called mixed mode (MM) pulses [6], have fast-risetimes and an asymmetrical wave shape similar to that of RS pulses. Pulses of the second type, called M-component-type ICC (M-ICC) pulses, are characterised by a slow risetime and a more or less symmetrical waveform.

The fourth and last category of pulses is that of classical MC pulses, which are superimposed on the CC that may follow some of the RSs of a flash.

In our data, the sample sizes of the four categories are considered as follows:

- 8 RS pulses,
- 59 MM ICC pulses,

- 17 M-ICC pulses, and
- 10 classical MC pulses.

The overall current waveforms and the simultaneously-measured electric field waveforms at 15 km distance for each of the two flashes are shown in Figs. 1 and 2. Two pulses for each pulse category, eight in total, will be used in Section 4 as a reference to validate model-predicted fields. These pulses are marked with arrows in Figs. 1 and 2 and they are labelled MM1, MM2, MICC1, MICC2, RS1, RS2, MC1, and MC2.

To improve the discernibility of the slow-varying ICC and the CC, a low-pass filter was applied to the overall current waveform. Fig. 3 shows the current waveforms of the two flashes after the application of a 1-kHz low-pass, zero-phase filter.

It can be seen in Fig. 3 that the initial stage of the flash that occurred on 4 August, at 23:52 starts at about 800 ms and lasts until about 1650 ms. The initial stage of the flash that occurred on 4 August, at 23:57 starts at about 650 ms and lasts until about 1220 ms. Both flashes included a CC (marked as CC in the figure), which occurred after the last RS of each flash.

It should be noted that the GPS was not working properly during these two flashes. Therefore, the current pulses and the associated electric field pulses were aligned manually by matching the times of the current peak and the associated field peak of the last RS for each flash. The error of the alignment was of the order of a few microseconds [7].

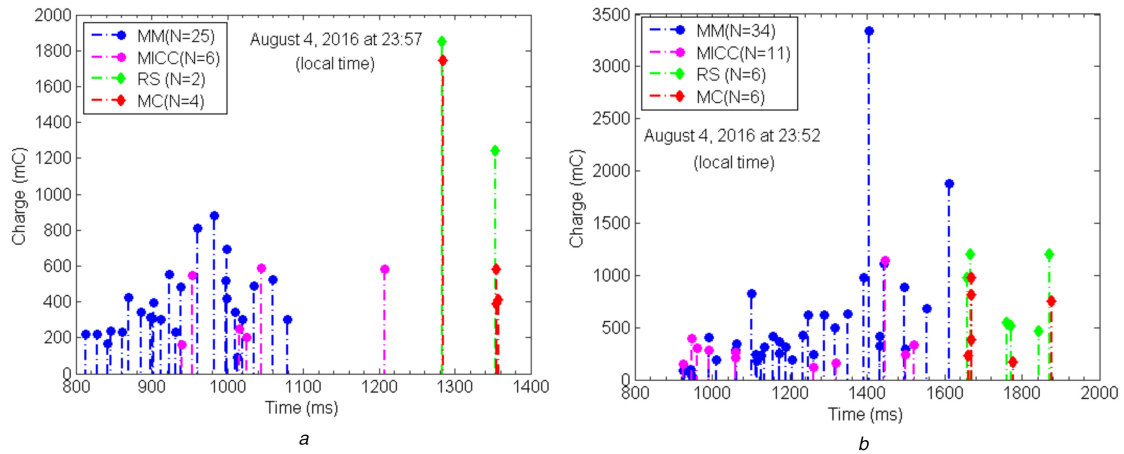


Fig. 4 Transferred charge associated with each pulse as a function of the time of occurrence in the flashes that occurred on 4 August 2016 at (a) 23:57, (b) on 23:52

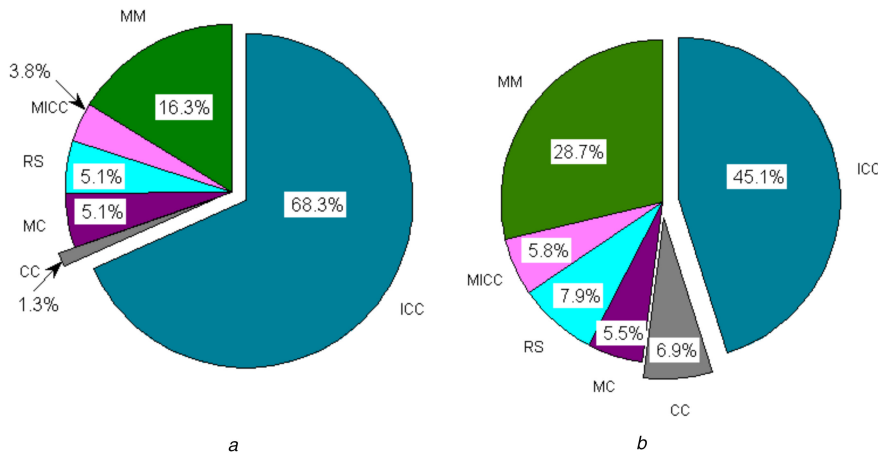


Fig. 5 Contribution of the different charge transfer modes to the total charge transferred to the ground (a) Flash that occurred on 4 August 2016 at 23:57, (b) Flash that occurred on 4 August 2016 at 23:52. Labels used in this figure are explained in Section 2.2

3 Characteristics of currents and charges associated with different charge transfer modes in upward flashes

3.1 Transferred charge associated with the four considered categories of pulses

The transferred charge is an important parameter of a lightning flash, since it is responsible for the thermal effects causing melting and burning through damages. Extensive use of composite materials in modern airplanes and wind turbine blades makes this parameter critical for the proper design of lightning protection systems [11].

Figs. 4a and b present the plots of the transferred charge associated with every pulse in the two flashes. The procedure used to compute the transferred charge is described in the Appendix. The amount of charge transferred by each type of pulse is shown by different markers: blue filled circles for MM pulses, pink-filled circles for MICC pulses, green diamond markers for RS pulses, and red diamond markers for MC pulses. One can see that, during both of the considered flashes, the MM pulses tend to transfer more charge than M-ICC pulses. Similarly, RS pulses tend to transfer more charge than classical MC pulses. The average charge transferred by M-ICC pulses for the two flashes was 0.35 C, while it was 0.65 C for classical MC pulses. Even though the average charge transferred by MM pulses was 0.47 C, which is only half of the average 1 C transferred by an RS, some MM pulses can transfer more charge than RS pulses (see Fig. 4b).

3.2 Contribution of different charge transfer modes to the total charge transferred to the ground

Fig. 5 presents the contribution of different charge transfer modes to the total charge transferred to the ground during each flash. It can be seen that the ICC is the largest of all the contributors to the overall transferred charge (68% for one of the flashes and 45% for the other one). Interestingly, MM pulses are the second largest contributor to the overall transferred charge, followed by RS, MC, MICC, and the CC. The high amount of charge transfer by MM pulses is essentially due to the relatively large number of these pulses, which originate from the attachment of rejuvenated or newly created branches to the ICC-carrying channel at low junction heights (<1 km) [6].

In both considered flashes, most of the charge was transferred during the initial stage of the upward flash (79.6% for the flash occurred on 4 August 2016 at 23:52 and 88.4% for the flash occurred on 4 August 2016 at 23:57, when the impulsive and steady-current charge transfers are combined).

Table 1 summarizes the amount of transferred charge associated with the different charge transfer modes in the two considered flashes.

3.3 Currents associated with the four considered categories of pulses

Table 2 presents a summary of the statistics, median (Med), arithmetic mean (AM) and range of variation (Min–Max), of the parameters of current and the electric field waveforms associated with the four categories of pulses. These parameters are

- 10–90% risetime RT.
- Current peak I_p .

- Full width at half maximum (FWHM), and
- Asymmetrical waveform coefficient (AsWC), which is a measure of the waveform symmetry defined as [5]

$$\text{AsWC} = \frac{\text{FWHM} - I_{50\% - 100\%}}{\text{FWHM}} \quad (1)$$

A fully symmetrical pulse is characterised by an AsWC of 1/2, while for asymmetrical impulsive waveforms (such as RS currents) the AsWC is close to 1.0.

From Table 2, one can see that both the median and the arithmetic mean for RT and for FWHM are much shorter for MM pulses and RS pulses than for M-ICC pulses and MC pulses. On the other hand, the parameters of the M-ICC pulses are very similar to those of classical MC pulses. M-ICC and classical MC pulses are characterised by risetimes and durations (FWHM) of several hundred microseconds, and peak currents of about 2 kA. The similarities are also found between MM and RS pulses, both of which are characterised by shorter risetimes, shorter durations, and higher peak currents. More information on the current waveform characteristics for the different pulse categories can be found in [5, 7].

4 Modeling of different charge transfer modes and calculating their electric fields

4.1 Modelling

The vertical electric fields associated with different charge transfer modes are calculated assuming a vertical channel above a perfectly-conducting ground. The field expression is given by [12, 13]

$$\begin{aligned} E_z(d, t) = & \frac{1}{2\pi\epsilon_0} \int_0^{H(t)} \frac{2z'^2 - d^2}{R^5(z')} \int_{R/c}^t i(z', \tau - \frac{R}{c}) d\tau dz' \\ & + \frac{1}{2\pi\epsilon_0} \int_0^{H(t)} \frac{2z'^2 - d^2}{cR^4(z')} i(z', t - R(z')/c) dz' \\ & - \frac{1}{2\pi\epsilon_0} \int_0^{H(t)} \frac{d^2}{c^2 R^3(z')} \frac{\partial i(z', t - R(z')/c)}{\partial t} dz' \end{aligned} \quad (2)$$

in which $i(z', t)$ is the current as a function of the position along the channel z' and the time t , c is the speed of light, d is the horizontal distance between the Sântis Tower and the field observation point, in this case, $d = 14.7$ km, $R = (d^2 + z'^2)^{1/2}$, and $H(t)$ is the radiating channel length. Based on the results of [14], an overall field correction factor of 2.0 to account for the presence of the 124-m tower and the mountainous propagation path was used in the simulations.

4.1.1 Current distribution in the RS and the mixed charge transfer modes: As discussed in [7], the characteristics of MM pulses are very similar to those of RSs. In this study, we use the same model for calculating the fields from both RSs and MM processes. The adopted model is the modified transmission line model with exponential current decay with height (MTLE) [15, 16], in which the current distribution is expressed as

$$\begin{aligned} i(z', t) &= i_0(t - z'/v)e^{-z'/\lambda} \quad z' \leq vt \\ i(z', t) &= 0 \quad z' > vt \end{aligned} \quad (3)$$

where v is the RS speed and λ is the current attenuation distance.

Current distribution given by (3) is assumed to apply to both the 124-m tower and the lightning channel attached to its top.

4.1.2 Current distribution in the MC and M-ICC pulses charge transfer modes: MCs and M-ICC pulses are modelled by a superposition of two current waves propagating without distortion: a downward incident current and an upward current reflected off the interface between the bottom of the lightning channel and the impedance seen by the lightning at the strike point [2, 17]. The distribution of the MC mode current along the ICC channel during the initial stage or the continuing-current channel after RSs is expressed as [2] (see (4)), where v_m is the velocity of the MC current wave, h_m is the height above the tower top of the junction point between the newly formed or reactivated branch and the ICC/CC carrying channel, and ρ_g is the reflection coefficient at the ground (recall that the presence of a tower is neglected in this study, except for the adjustment factor of 2 in the calculated fields).

Table 1 Amount of transferred charge (in coulomb) associated with the different charge transfer modes in the two considered upward flashes (unit: coulomb)

Flash ID	Total charge	Impulsive current components				Steady current components	
		MM	MICC	RS	MC	ICC	CC
4 August 2016 at 23:52	61.95	17.8	3.6	4.9	3.4	27.95	4.3
4 August 2016 at 23:57	60.28	9.8	2.3	3.1	3.1	41.18	0.8

Table 2 Characteristics of the current waveforms associated with the four categories of pulses

Parameter	Statistics	MM	MICC	RS	MC
		(N = 59)	(N = 17)	(N = 8)	(N = 10)
RT, μ s	Med	4.56	83.12	0.74	193.06
	AM	5.84	124.71	0.95	203.98
	Min.–Max.	0.66–27.62	6.30–400.57	0.58–1.86	40–429.77
I_p , kA	Med	3.93	1.51	9.82	1.63
	AM	4.78	2.04	10.68	1.86
	Min.–Max.	1.05–18.02	0.93–7.08	6.20–18.41	0.65–4.47
FWHM, μ s	Med	53.44	108.99	31.15	242.58
	AM	61.90	143.79	36.00	257.92
	Min.–Max.	22.99–197.66	28.26–378.49	21.42–61.32	170.47–368.69
AsWC (relative units)	Med	0.93	0.67	0.98	0.65
	AM	0.92	0.66	0.98	0.61
	Min.–Max.	0.802–0.996	0.486–0.798	0.952–0.994	0.376–0.727

Min: minimum value, Max: maximum value.

Med: median value, AM: arithmetic mean value.

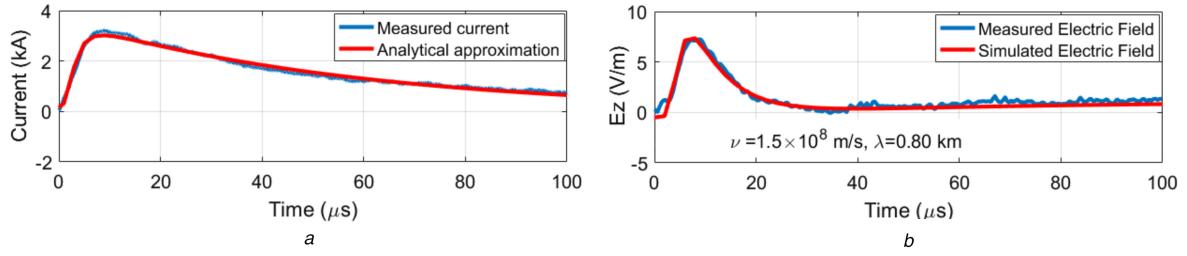


Fig. 6 Current and electric field waveforms at 15 km for MM1
(a) Current, (b) Electric field

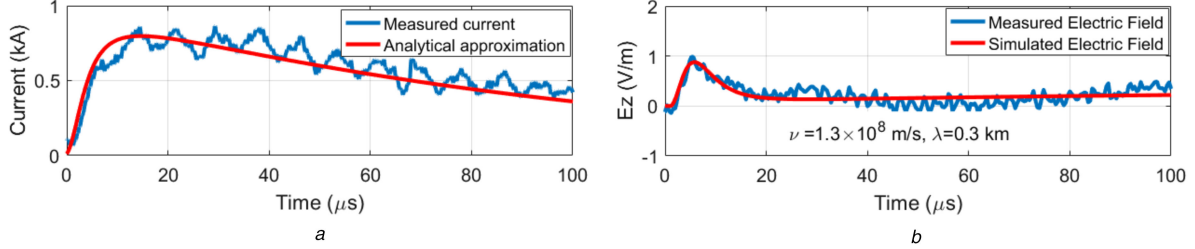


Fig. 7 Current and electric field waveforms at 15 km for MM2
(a) Current, (b) Electric field

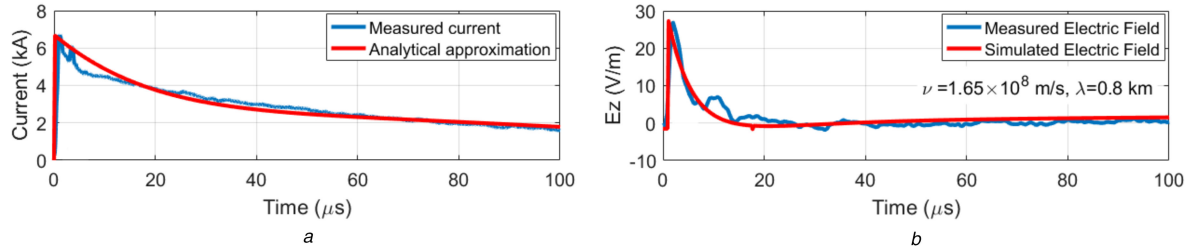


Fig. 8 Current and electric field waveforms at 15 km for RS1
(a) Current, (b) Electric field

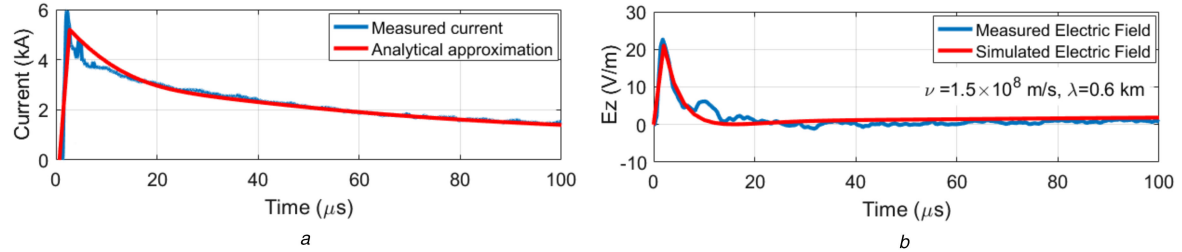


Fig. 9 Current and electric field waveforms at 15 km for RS2
(a) Current, (b) Electric field

4.2 Simulation results and comparison with experimental data

Eight pulses (two of each type) identified in Figs. 1 and 2 were used to compare the measurements with the simulation results. For each pulse, the measured current was represented analytically by the sum of two Heidler's functions with parameters evaluated using a genetic algorithm [18]. The parameters of the models, namely ν and λ for RSs and MM pulses, and ν_m , h_m , and ρ_g for MCs and M-ICC pulses, were adjusted to match the simulation results with the experimental data.

4.2.1 RSs and MM pulses: Figs. 6b–9b present the simulation results for the selected two RSs and two MM pulses, along with the experimental waveforms.

From these figures, one can see that the calculated fields for both RSs and MM pulses are in excellent agreement with the

measured waveforms. The model parameters ν and λ providing the best match between computed and measured fields are given in the figures and in Table 3.

The velocities of the four pulses range from 1.3×10^8 to 1.65×10^8 m/s, which are in the range of the experimentally-observed RS speeds (e.g. [19, 20]). However, the exponential attenuation height constants for the four pulses range from 0.3 to 0.8 km, lower than the value of 2.0 km suggested in [15, 21].

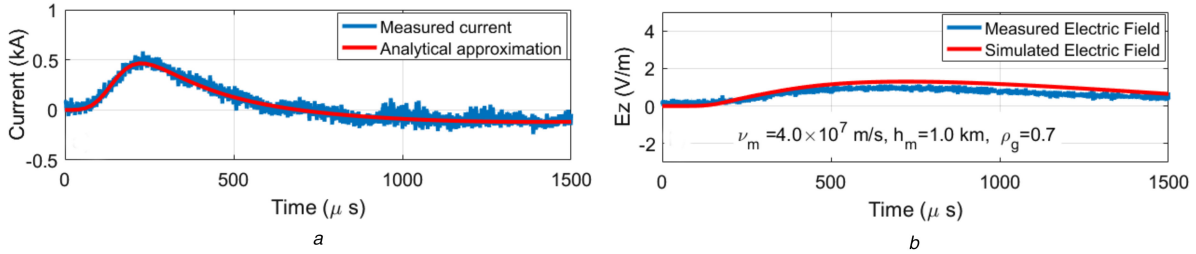
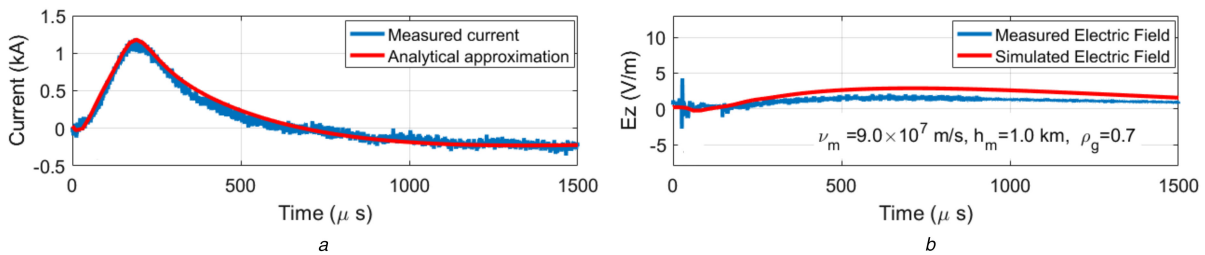
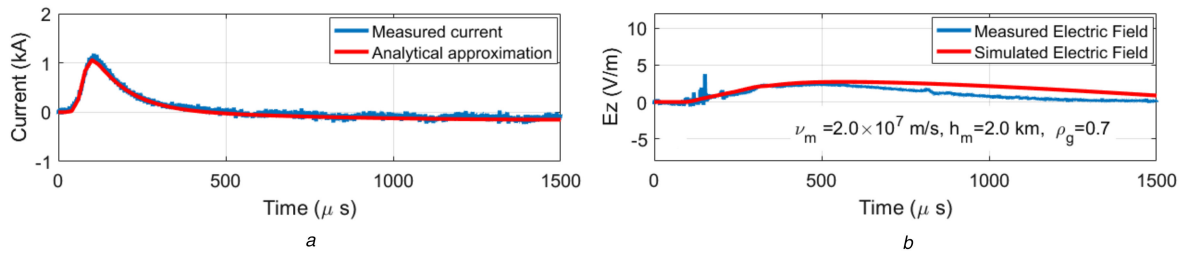
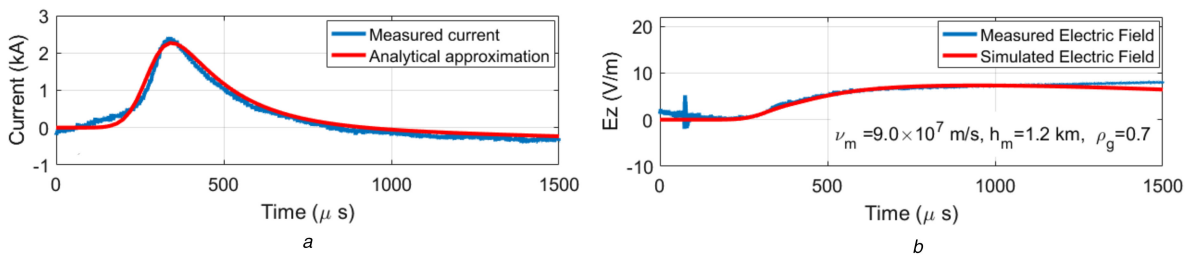
The good agreement between the electric fields predicted by the MTLE RS model and the measured field waveforms for MM pulses supports the hypothesis that the charge transfer mode resulting in MM pulses is similar to that of RSs.

4.2.2 MCs and M-ICC pulses: Figs. 10b–13b present the simulation results for MCs and M-ICC pulses, which are believed to be manifestations of the same mode of charge transfer to the

$$\begin{aligned}
 i(z', t) &= i(h_m, t - (h_m - z')/\nu_m) & t < h_m/\nu_m \\
 i(z', t) &= i(h_m, t - (h_m - z')/\nu_m) + i(h_m, t - (h_m + z')/\nu_m)\rho_g & t \geq h_m/\nu_m
 \end{aligned} \tag{4}$$

Table 3 Parameters derived from matching simulated and measured fields

Event ID	$v, \times 10^8$ m/s	H , km	λ , km	Event ID	$v_m, \times 10^7$ m/s	h_m , km	ρ_g
MM1	1.50	8.00	0.80	MC1	4.00	1.00	0.70
MM2	1.30	8.00	0.30	MC2	9.00	1.00	0.70
RS1	1.65	8.00	0.80	MICC1	2.00	2.00	0.70
RS2	1.50	8.00	0.60	MICC2	9.00	1.20	0.70

**Fig. 10** Current and electric field waveforms at 15 km for MC1
(a) Current, (b) Electric field**Fig. 11** Current and electric field waveforms at 15 km for MC2
(a) Current, (b) Electric field**Fig. 12** Current and electric field waveforms at 15 km for MICC1
(a) Current, (b) Electric field**Fig. 13** Current and electric field waveforms at 15 km for MICC2
(a) Current, (b) Electric field

ground. In the same figures, we have plotted the observed waveforms. The model parameters (v_m , h_m and ρ_g) that provide the best match between computed and measured fields are given in Figs. 10b–13b.

From Figs. 10b and 11b, one can see that the simulated fields for MC pulses are in excellent agreement with the corresponding measured fields. Although there are slight deviations in the tail of the waveforms (after about 750 μ s for MICC1 and after 1250 μ s for MICC2 in Figs. 12b and 13b, respectively), the simulated fields and the corresponding measured waveforms for M-ICC pulses are also in good agreement with each other. Fast microsecond-scale pulses can be observed before the slowly varying recorded electric

field of the MC and MICC electric field waveforms. These fast pulses are presumably due to the junction process between the newly formed or reactivated branch and the ICC or CC carrying channel (see [7, 22] for more information).

The model parameters providing the best match to the measured fields for each pulse are shown in Table 3. The propagation speeds for the four pulses range from 2.0×10^7 to 9.0×10^7 m/s, which are in the range of speeds expected for MCs according to [2, 23]. The junction point heights for MCs and M-ICC pulses range from 1.0 to 2.0 km, which are consistent with the study presented in [6].

The good agreement between the vertical electric fields predicted by the MC model and the measured field waveforms for

M-ICC pulses supports the assumption that their charge transfer mode is similar to that of MCs.

5 Conclusions

In this paper, we presented an analysis of different charge transfer modes in upward negative flashes. The experimental data for the analysis comprised a total of 94 pulses that occurred during two upward negative flashes recorded at the Sântis Tower. The pulses included 59 MM ICC pulses, 17 M-ICC pulses, 8 RS pulses, and 10 classical MC pulses.

The average charges transferred to the ground by MM, M-ICC, RS, and classical MC pulses were 0.47, 0.35, 1.0, and 0.65 C, respectively. It was found that the initial stage of the flash was responsible for the largest share in the total amount of charge transferred to the ground. In both considered flashes, at least 79.6% of the total charge was indeed transferred during the initial stage of the upward flash.

Simulation results for the electric fields associated with the considered charge transfer modes were presented and discussed. RS and MM pulses were simulated adopting the MTLE model, while MCs and M-ICC pulses were simulated using the model of Rakov [2]. The simulated results were found to be in good agreement with measurements of electric fields performed at 15 km from the Sântis Tower.

The inferred velocities for the MCs and M-ICC pulses used to obtain the best match between experimental data and simulations range from 2.0×10^7 to 9.0×10^7 m/s, and the corresponding junction point heights range from 1.0 to 2.0 km. The inferred pulse velocities for RSs and MM pulses range from 1.3×10^8 to 1.65×10^8 m/s. The inferred current attenuation distances of the MTLE model obtained in this study range from 0.3 to 0.8 km, which are lower than the value of 2 km previously suggested for RSs in downward flashes.

The obtained results support the assumption that the mode of charge transfer to the ground giving rise to sharp pulses superimposed on steady currents is similar to that of the leader/RS mode. The results are also in support of the generally assumed similarity between M-ICC pulses and classical MCs.

6 Acknowledgments

Financial supports from the Swiss National Science Foundation (Project No. 200021_147058) and the European Union's Horizon 2020 research and innovation programme (grant agreement. no 737033-LLR) are acknowledged. It is also supported by the China Scholarship Council (CSC).

7 References

- [1] Malan, D., Collens, H.: 'Progressive lightning. III. The fine structure of return lightning strokes', *Proc. R. Soc. Lond. A Math. Phys. Sci.*, 1937, **1937**, pp. 175–203, doi: 10.1098/rspa.1937.0175
- [2] Rakov, V.A., Thottappillil, R., Uman, M.A., *et al.*: 'Mechanism of the lightning m component', *J. Geophys. Res.*, 1995, **100**, pp. 25701–25710
- [3] He, L., Rachidi, F., Azadifar, M., *et al.*: 'Electromagnetic fields associated with the m-component mode of charge transfer', *J. Geophys. Res. Atmos.*, 2019, **124**, pp. 1–19, doi: 10.1029/2018JD029998
- [4] Zhang, Y., Zhang, Y., Xie, M., *et al.*: 'Characteristics and correlation of return stroke, m component and continuing current for triggered lightning', *Electr. Power Syst. Res.*, 2016, **139**, pp. 10–15, doi: 10.1016/j.epr.2015.11.024
- [5] He, L., Azadifar, M., Rachidi, F., *et al.*: 'An analysis of current and electric field pulses associated With upward negative lightning flashes initiated from the Sântis tower', *J. Geophys. Res. Atmos.*, 2018, **123**, (8), pp. 4045–4059
- [6] Zhou, H., Rakov, V.A., Diendorfer, G., *et al.*: 'A study of different modes of charge transfer to ground in upward lightning', *J. Atmos. Terr. Phys.*, 2015, **125–126**, pp. 38–49, doi: <http://dx.doi.org/10.1016/j.jastp.2015.02.008>
- [7] Azadifar, M., Rachidi, F., Rubinstein, M., *et al.*: 'Fast initial continuous current pulses versus return stroke pulses in tower-initiated lightning', *J. Geophys. Res. Atmos.*, 2016, **121**, (11), pp. 6425–6434, doi: 10.1002/2016jd024900
- [8] He, L., Azadifar, M., Quanxin, L., *et al.*: 'Modeling of different charge transfer modes in upward flashes constrained by simultaneously measured currents and fields'. 2018 IEEE Int. and Asia-Pacific Symp. on Electromagnetic Compatibility (EMC/APEMC), Singapore, 2018, pp. 403–407, doi: 10.1109/ISEMC.2018.8393809
- [9] Romero, C., Rachidi, F., Paolone, M., *et al.*: 'Statistical distributions of lightning currents associated with upward negative flashes based on the data

- collected at the Sântis (EMC) tower in 2010 and 2011', *IEEE Trans. Power Deliv.*, 2013, **28**, (3), pp. 1804–1812
- [10] Azadifar, M., Paolone, M., Pavanello, D., *et al.*: 'An update on the characteristics of positive flashes recorded on the Sântis tower'. 2014 Int. Conf. on Lightning Protection (ICLP), Shanghai, China, 2014
- [11] Smorgonskiy, A., Rachidi, F., Rubinstein, M., *et al.*: 'Are standardized lightning current waveforms suitable for aircraft and wind turbine blades made of composite materials?', *IEEE Trans. Electromagn. Compat.*, 2017, **59**, (4), pp. 1320–1328
- [12] Uman, M.A., McLain, D.K., Krider, E.P.: 'The electromagnetic radiation from a finite antenna', *Am. J. Phys.*, 1975, **43**, (1), pp. 33–38
- [13] Rubinstein, M., Uman, M.A.: 'Methods for calculating the electromagnetic fields from a known source distribution: application to lightning', *IEEE Trans. Electromagn. Compat.*, 1989, **31**, (2), pp. 183–189
- [14] Li, D., Azadifar, M., Rachidi, F., *et al.*: 'On lightning electromagnetic field propagation along an irregular terrain', *IEEE Trans. Electromagn. Compat.*, 2016, **58**, (1), pp. 161–171
- [15] Nucci, C.A., Mazzetti, C., Rachidi, F., *et al.*: 'On lightning return stroke models for LEMP calculations'. 19th Int. Conf. on Lightning Protection (ICLP), Graz, Austria, 1988
- [16] Rachidi, F., Nucci, C.: 'On the master, uman, linin, standler and the modified transmission line lightning return stroke current models', *J. Geophys. Res. Atmos.*, 1990, **95**, (D12), pp. 20389–20393
- [17] Rakov, V.A., Crawford, D.E., Rambo, K.J., *et al.*: 'M-component mode of charge transfer to ground in lightning discharges', *J. Geophys. Res. Atmos.*, 2001, **106**, (D19), pp. 22817–22831
- [18] Chandrasekaran, K., Puneekar, G.S.: 'Use of genetic algorithm to determine lightning channel-base current-function parameters', *IEEE Trans. Electromagn. Compat.*, 2014, **56**, (1), pp. 235–238
- [19] Carvalho, F.L., Uman, M.A., Jordan, D.M., *et al.*: 'Frequency domain analysis of triggered lightning return stroke luminosity velocity', *J. Geophys. Res. Atmos.*, 2017, **122**, (4), pp. 2334–2350
- [20] Rakov, V.A.: 'Lightning return stroke speed', *J. Lightning Res.*, 2007, **1**, pp. 80–89
- [21] Nucci, C., Rachidi, F.: 'Experimental validation of a modification to the transmission line model for LEMP calculation'. 8th Symp. and Technical Exhibition on Electromagnetic Compatibility, Zurich, Switzerland, 1989
- [22] Tran, M., Rakov, V., Ngai, T., *et al.*: 'Microsecond-scale electric field pulses associated with lightning m-components'. AGU Fall Meeting Abstracts, San Francisco, CA, USA, 2013
- [23] Jordan, D.M., Idone, V.P., Orville, R.E., *et al.*: 'Luminosity characteristics of lightning m components', *J. Geophys. Res. Atmos.*, 1995, **100**, (D12), pp. 25695–25700
- [24] Fisher, R., Schnetzer, G., Thottappillil, R., *et al.*: 'Parameters of triggered-lightning flashes in Florida and Alabama', *J. Geophys. Res. Atmos.*, 1993, **98**, (D12), pp. 22887–22902

8 Appendix

8.1 Calculation of the transferred charge associated with current pulses

In this Appendix, we describe the procedure adopted in this paper for the evaluation of the transferred charge associated with different charge transfer modes in an upward flash (see Fig. 14).

Fig. 14a shows schematically a pulse, denoted as ICCP, superimposed on the ICC, whether MM or MICC. I_{ICC} represents the continuous current level at the onset of the ICCP. I_{ICCP} denotes the peak of the pulse, relative to I_{ICC} . T_{ICCP} represents the duration of the pulse, defined as the interval from the onset of the pulse to a point at which the trailing edge of the pulse becomes indistinguishable from the I_{ICC} . The charge transferred during the pulse corresponds to the integral shown by the pink-shaded area in the figure.

RSs, which occur after the extinction of the ICC, if any, are preceded by an essentially no-current time interval. Therefore, the charge transferred by an RS pulse, which is not followed by any CC can be evaluated straightforwardly. Fig. 14b shows schematically an RS pulse followed by a CC and MC pulses. I_{RS} denotes the magnitude of the RS pulse. The beginning of the CC, identified in the figure with a small solid green circle, corresponds to the local minimum from the slowly decaying tail of the preceding RS. This point is also assumed as the ending point of the RS. T_{RS} represents the duration of the RS. The charge transferred by the RS (Q_{RS}) in this case is the time integral (during T_{RS}) of the RS pulse above the time-axis (shown by the black-shaded area). I_M represents the peak of the first MC pulse, relative to I_{CC} , which represents the CC level at the onset of the MC. T_M represents the duration of the MC which is the time interval from the beginning of the MC (identified as the initial deflection from the preceding

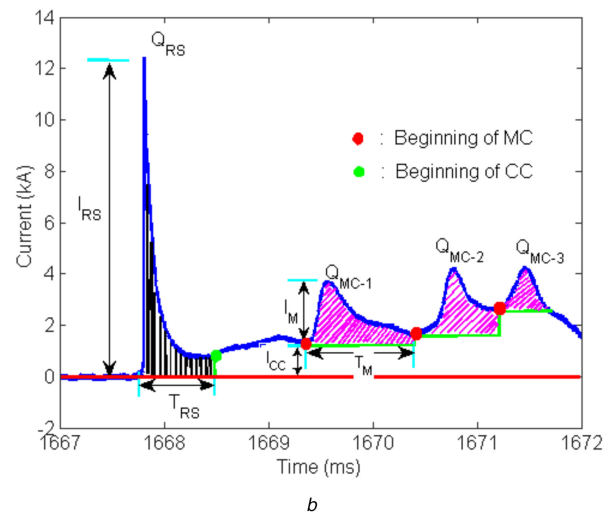
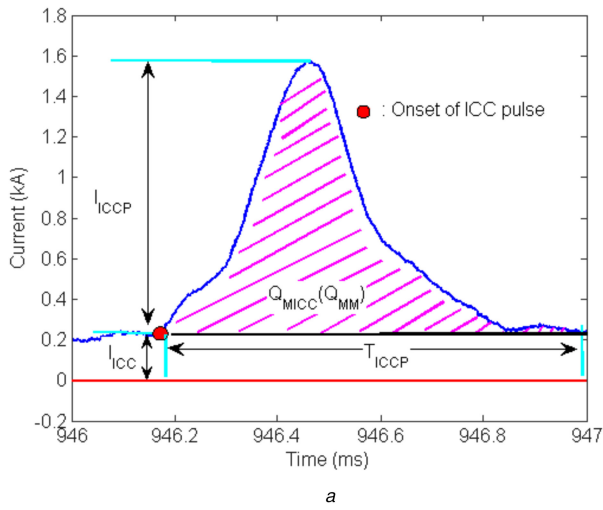


Fig. 14 Estimation of the charge transferred to the ground
 (a) For MM and M-ICC pulses, (b) For RS and MC pulses

I_{CC} [24] shown with the small solid red circle) to either the beginning of the next MC, or to the point at which the MC current falls to its initial value. The charge transferred by the MC (Q_M) is

the time integral of the MC pulse above the I_{CC} during T_M (the pink-shaded area in Fig. 14b). The evaluation of the charge in two additional MC pulses is also illustrated in Fig. 14b.